# Transient, Linear Dynamics of a Stably Stratified Shear Flow with Thermal Forcing and a Critical Level

JONG-JIN BAIK AND HONG-SUB HWANG

*Department of Environmental Science and Engineering, Kwangju Institute of Science and Technology, Kwangju, Korea*

HYE-YEONG CHUN

*Department of Atmospheric Sciences and Global Evironmental Laboratory, Yonsei University, Seoul, Korea*

(Manuscript received 22 May 1997, in final form 6 February 1998)

ABSTRACT

The transient, linear response of a stably stratified atmosphere to thermal forcing in the presence of a critical level is investigated analytically using the Green's function method. The prescribed thermal forcing is located below or across a critical level. The target solution is for the finite-depth steady forcing, but intermediate solutions to the line-type pulse forcing, finite-depth pulse forcing, and line-type steady forcing are analyzed in some detail because these solutions give some insight into the basic dynamics of the response to the target forcing.

The responses to the pulse forcings exhibit the moving mode whose center travels downstream with a speed of the basic-state wind. In the vicinity of the initial forcing, gravity waves are attenuated across the critical level. In response to the line-type pulse forcing, after some time the magnitude of the perturbation vertical velocity at the center of the moving mode remains almost unchanged with time. The transient critical level is a function of the horizontal location and time. In response to the finite-depth pulse forcing, after some time the magnitude of the perturbation vertical velocity at the line that connects the centers of the moving modes at the forcing top and bottom decreases with time due to the geometric expansion of the line. In responses to the steady forcings, the stationary mode as well as the moving mode appear. The origin of the stationary mode is very small-amplitude waves with zero or near-zero horizontal phase velocities in the pulse forcings. These waves work constructively to be perceptible in response to the steady forcings. The stationary mode is almost entirely absorbed at the critical level, and the dynamics of the moving modes in the pulse and steady forcing cases are similar to each other. It is shown that adding a widespread heating (cooling) term eventually yields a steady-state field in the stationary mode. Unlike the steady-state case, there is a gradual decrease of the momentum flux from the thermal forcing top to the critical level. The moving mode can transport a small amount of the momentum flux above the critical level.

## 1. Introduction

There are numerous interesting mesoscale meteorological phenomena that are forced by diabatic heating or cooling. These include thunderstorm outflows, squall line circulation, heat islands, mesoscale solitary waves, and so on. Thunderstorm cold-air outflows, which are produced by the evaporative cooling of falling precipitation in the subcloud layer and spread out along the surface, have been known to trigger successive convective cells in multicellular storms, maintain supercell storms, and promote merger between existing convective clouds [see references in Droegemeier and Wilhelmson (1987)]. Midlatitude squall lines frequently exhibit a critical level (a level at which the basic-state horizontal wind speed is equal to the propagation speed of a disturbance) near 6 km above the surface in a reference frame moving with the system (Ogura and Liou 1980; Bluestein and Jain 1985; Wyss and Emanuel 1988). The deep convection across the critical level can have a significant effect on the dynamics of squall lines (Lin 1987). Heat islands produce upward motion downwind and precipitation tends to increase downwind of heat islands (Garstang et al. 1975; Changnon et al. 1991). Mesoscale solitary waves can be originated near a region of deep convection (Lin and Goff 1988), propagate a long distance, and trigger convection.

Gravity waves in the atmosphere play important dynamical roles in the spectral energy transfer, the transport of momentum and energy from one region to another, and the triggering of instabilities that cause severe convective systems to develop (Hooke 1988). There are several numerical modeling studies to examine the role of gravity waves in the circulation that develops around

*Corresponding author address:* Prof. Jong-Jin Baik, Department of Environmental Science and Engineering, Kwangju Institute of Science and Technology, 572 Sangam-dong, Kwangsan-ku, Kwangju 506-712, Korea.
E-mail: jjbaik@aromi.kjist.ac.kr

diabatic forcing. Yang and Houze (1995) suggested that the multicellular structure of a midlatitude squall line is associated with gravity waves generated by convection. Pandya and Durran (1996) showed that the transient response of gravity waves induced by thermal forcing is crucial to the squall line circulation and that the response to thermal forcing explains almost all the features of the squall line circulation.

The problem of thermally induced mesoscale circulation can be accessible theoretically by investigating the atmospheric response to specified thermal forcing. Along this line of research, much of the basic dynamics behind complex but fascinating thermally induced mesoscale phenomena have been understood during the past decades. In particular, the two-dimensional, linear, steady-state response of a stably stratified flow to thermal forcing has been examined extensively. Olfe and Lee (1971) studied urban heat island convection effects on temperature and velocity fields by performing flow calculations in a uniform basic-state flow where the heating is diffusively produced from the surface source. They showed that there is downward motion on the upstream side of and over heat islands and upward motion on the downstream side. This is consistent with observations (Angell et al. 1971; Garstang et al. 1975). Smith and Lin (1982) examined the response of a stratified airstream to combined thermal and orographic forcing in a uniform basic-state flow. They found that in order to avoid a net heating problem in a two-dimensional, linear, steady-state, inviscid flow system, a widespread cooling term should be included in the thermal forcing and that the phase relationship between the heating and the induced vertical displacement is negative. This negative phase relationship helps explain the reduced mountain waves in the moist atmosphere (e.g., Fraser et al. 1973; Barcilon et al. 1980) and downward motion over heat islands (e.g., Garstang et al. 1975). Raymond (1986) studied the response of a stratified atmosphere to a moving heat source as a model for understanding organized moist convection. He showed that the response fields are strongly dependent upon the ratio of the vertical wavelength of forced gravity waves to the heating depth.

When the vertical shear of the basic-state horizontal wind with or without a critical level is included, the linear, steady-state response to thermal forcing becomes different from that of the uniform flow case. Baik (1992) showed that the magnitude of the perturbation vertical velocity is larger in the critical-level free shear flow case than in the uniform flow case. This is because the basic-state wind shear can be a source of the perturbation wave energy. It is well known that internal gravity waves passing through a critical level are attenuated exponentially if the Richardson number of the basic-state flow is greater than ¼ (Booker and Bretherton 1967). In a study of the response of a stably stratified shear flow with a critical level to diabatic heating, Lin (1987) found that in response to heating located below the critical level, most of the perturbation wave energy is absorbed at the critical level and that the low-level vertical velocity near the heating center can be either positive or negative depending on the Richardson number of the basic-state flow and the heating depth. He also found that in response to heating located across the critical level, the vertical velocity near the heating center is almost always positive for a wide range of Richardson numbers. The upward motion at the heating base is important in maintaining existing convection. In a study of the three-dimensional response of a shear flow with a critical level to elevated heating, Lin and Li (1988) regarded the V-shaped regions of midlatitude convective storm tops as a gravity wave phenomenon.

Compared with research on the linear, steady-state response to thermal forcing, research on the linear, time-dependent (transient) response has been restricted because of more mathematical complexity. Lin and Smith (1986) addressed the problem of the transient response of a stably stratified uniform basic-state flow to a heat source. By viewing a maintained heat source as a train of heat pulses, they showed that the response exhibits a region of positive displacement moving downstream and negative displacements near the stationary heat source as a steady-state is approached. This clarifies the strange negative phase relationship between the heating and the induced vertical displacement in the steady-state problem. With group velocity arguments, Bretherton (1988) examined the response of a stratified uniform basic-state flow to internal heat or mass sources. He presented the generalized condition for a steady-state response to a distributed maintained heat source, that is, the heat source distribution has no projection onto the modes of zero group velocity. The transient response of a quiescent atmosphere to heat sources was studied by Nicholls et al. (1991) with some comparison between rigid-lid and semi-infinite cases (Pandya et al. 1993). However, a problem that still remains unsolved so far is the problem of the linear, transient response of a stably stratified shear flow with a critical level to thermal forcing.

In this paper, in order to further enhance our understanding of basic dynamics behind thermally induced mesoscale circulation, we will theoretically investigate the transient response of a stably stratified shear flow with thermal forcing and a critical level. Of particular interest in this study is the situation in which diabatic cooling is located from the surface to a certain height below a critical level, representing the evaporative cooling of falling precipitation in the subcloud layer, and the situation in which diabatic heating is located across a critical level, representing latent heating due to moist convection. Under these circumstances, the effects of critical level and wind shear on thermally induced gravity waves and the resultant gravity wave response field will be examined in detail. In section 2, analytical solutions to the governing equation set in a semi-infinite domain are obtained using the Green's function method.

To get solution to the finite-depth steady thermal forcing (target forcing), solution to the line-type pulse forcing is obtained first. In section 3, results from intermediate solutions (line-type pulse forcing, finite-depth pulse forcing, and line-type steady forcing) as well as target solution (finite-depth steady forcing) are discussed in detail because intermediate solutions provide some insight into the basic dynamics of the response to the finite-depth steady forcing. It will be shown that some limiting cases of our solutions indeed reproduce the steady-state solutions obtained by previous studies. This convinces the generality of our transient solutions presented in this study. In section 4, summary and conclusions follow.

## 2. Governing equations and solutions

We consider a two-dimensional, linearized, hydrostatic, nonrotating, inviscid, and Boussinesq fluid system. The equations governing perturbations in a basic-state horizontal wind with diabatic forcing can be expressed by

$$\frac{\partial u}{\partial t} + U\frac{\partial u}{\partial x} + w\frac{dU}{dz} = -\frac{\partial \pi}{\partial x}, \tag{1}$$

$$\frac{\partial \pi}{\partial z} = b, \tag{2}$$

$$\frac{\partial b}{\partial t} + U\frac{\partial b}{\partial x} + N^2 w = \frac{g}{c_p T_0} q, \tag{3}$$

$$\frac{\partial u}{\partial x} + \frac{\partial w}{\partial z} = 0. \tag{4}$$

Here, $u$ is the perturbation horizontal velocity, $w$ the perturbation vertical velocity, $\pi$ the perturbation kinematic pressure, $b$ the perturbation buoyancy, $U$ the basic-state horizontal wind, $N$ the buoyancy frequency, $g$ the gravitational acceleration, $c_p$ the specific heat of air at constant pressure, $T_0$ the basic-state temperature, and $q$ the diabatic forcing. In this study, the basic-state wind is given by

$$U(z) = U_0 - \alpha z, \tag{5}$$

where $U_0$ ($>0$) is the basic-state wind at the surface and $\alpha$ ($>0$) the vertical wind shear. The critical level is located at $z = U_0/\alpha$. The target diabatic forcing in this study is the finite-depth steady forcing that is located from the surface to a certain height below a critical level or located across a critical level. Equations (1)–(4) can be combined into a single equation for the perturbation vertical velocity

$$\left(\frac{\partial}{\partial t} + U\frac{\partial}{\partial x}\right)^2 \frac{\partial^2 w}{\partial z^2} + N^2 \frac{\partial^2 w}{\partial x^2} = \frac{g}{c_p T_0}\frac{\partial^2 q}{\partial x^2}. \tag{6}$$

To solve (6), we first seek a solution to the line-type pulse forcing given by

$$q(x, z, t) = q_0 \frac{a^2}{x^2 + a^2}\delta(z - \xi)\delta(t), \tag{7}$$

where $q_0$ is the amplitude of the diabatic forcing, $a$ the half-width of the bell-shaped function, $\delta$ the Dirac delta function, and $\xi$ the height at which the line-type forcing exists. Taking the Fourier transform in $x$ ($x \to k$) and Laplace transform in $t$ ($t \to s$) of (6) yields

$$\frac{\partial^2 \hat{w}}{\partial z^2} + \frac{N^2 (ik)^2}{(s + ikU)^2}\hat{w} = \frac{g q_0 a (ik)^2 e^{-ak}}{c_p T_0 (s + ikU)^2}\delta(z - \xi). \tag{8}$$

Note that unlike the steady-state, critical-level case (Lin 1987; Lin and Chun 1991; Chun and Lin 1995), the transient, critical-level case in (8) contains no singularity because of $\mathrm{Re}(s) > 0$. With an introduction of the perturbation streamfunction $\varphi$ defined by $u = \partial\varphi/\partial z$ and $w = -\partial\varphi/\partial x$, (8) can be rewritten as

$$\frac{\partial^2 \hat{\varphi}}{\partial z^2} + \frac{N^2 (ik)^2}{(s + ikU)^2}\hat{\varphi} = -\frac{g q_0 a (ik) e^{-ak}}{c_p T_0 (s + ikU)^2}\delta(z - \xi). \tag{9}$$

The general solution of (9) is

$$\hat{\varphi}_1(k, z, s) = A_1(k, s)(s + ikU)^{1/2 + i\mu} + B_1(k, s)(s + ikU)^{1/2 - i\mu} \quad \text{for } 0 \le z \le \xi, \tag{10a}$$

$$\hat{\varphi}_2(k, z, s) = A_2(k, s)(s + ikU)^{1/2 + i\mu} + B_2(k, s)(s + ikU)^{1/2 - i\mu} \quad \text{for } z > \xi. \tag{10b}$$

Here, $\mu = (N^2/\alpha^2 - \frac{1}{4})^{1/2} = (\mathrm{Ri} - \frac{1}{4})^{1/2}$, where Ri is the Richardson number defined by $N^2/\alpha^2$. The four unknown coefficients $A_1(k, s)$, $B_1(k, s)$, $A_2(k, s)$, and $B_2(k, s)$ can be determined by imposing lower and upper boundary conditions and interface conditions. The flat bottom boundary condition [$\hat{\varphi}_1(k, 0, s) = 0$] and the upper radiation condition (Booker and Bretherton 1967), which require $A_2(k, s) = 0$, are used. Two interface conditions at $z = \xi$ are obtained by integrating (9) twice from $z = \xi^-$ to $\xi^+$. That is,

$$\frac{\partial \hat{\varphi}_2}{\partial z} - \frac{\partial \hat{\varphi}_1}{\partial z} = \bar{v}\frac{g q_0 a (ik) e^{-ak}}{c_p T_0 (s + ikU)^2} \quad \text{at } z = \xi, \tag{11a}$$

$$\hat{\varphi}_2 - \hat{\varphi}_1 = 0 \quad \text{at } z = \xi. \tag{11b}$$

After these conditions are applied to (10), the solution for the perturbation streamfunction in transformed space follows:

$$\hat{\varphi}_1(k, z, s) = C_1 e^{-ak}(s + ikU_\xi)^{-3/2 - i\mu}(s + ikU)^{1/2 + i\mu} - C_1 e^{-ak}(s + ikU_\xi)^{-3/2 - i\mu}(s + ikU_0)^{2i\mu} \times (s + ikU)^{1/2 - i\mu} \quad \text{for } 0 \le z \le \xi, \tag{12a}$$

$$\hat{\varphi}_2(k, z, s) = C_1 e^{-ak}(s + ikU_\xi)^{-3/2 + i\mu}(s + ikU)^{1/2 - i\mu} - C_1 e^{-ak}(s + ikU_\xi)^{-3/2 - i\mu}(s + ikU_0)^{2i\mu} \times (s + ikU)^{1/2 - i\mu} \quad \text{for } z > \xi, \tag{12b}$$

where $C_1 = igq_0a/(2c_pT_0\alpha\mu)$ and $U_\xi$ is the basic-state wind at $z = \xi$. The second term on the right-hand side of (12) results from the flat bottom boundary condition. Taking the inverse Laplace transform in $s$ ($s \to t$) and inverse Fourier transform in $k$ ($k \to x$) of (12) gives, after some manipulations using the convolution theorem and contour integral method when performing the inverse Laplace transform, the solution for the perturbation streamfunction in physical space:

$$\varphi_1(x,z,t) = \mathrm{Re}\{C_1(B\xi)^{-3/2-i\mu}(BZ)^{1/2+i\mu} - C_1(B\xi)^{-3/2-i\mu}(B0)^{2i\mu}(BZ)^{1/2-i\mu}\} \quad \text{for } 0 \le z \le \xi, \tag{13a}$$

$$\varphi_2(x,z,t) = \mathrm{Re}\{C_1(B\xi)^{-3/2+i\mu}(BZ)^{1/2-i\mu} - C_1(B\xi)^{-3/2-i\mu}(B0)^{2i\mu}(BZ)^{1/2-i\mu}\} \quad \text{for } z > \xi, \tag{13b}$$

where $(B\xi) = a - i(x - U_\xi t)$, $(B0) = a - i(x - U_0 t)$, and $(BZ) = a - i(x - Ut)$. We do not further reduce (13) [also (14) and (15)] to a more compact form in order to emphasize the solution part that would be obtained if the infinite domain were considered and the solution part due to the flat bottom boundary condition. Evaluating the real part of (13) yields

$$\varphi_1(x,z,t) = C_2R_\xi^{-3/2}R^{1/2}e^{\mu(\theta_\xi-\theta)}\sin\left[\frac{\theta}{2} - \frac{3\theta_\xi}{2} - \mu\ln\left(\frac{R_\xi}{R}\right)\right] - C_2R_\xi^{-3/2}R^{1/2}e^{\mu(\theta_\xi+\theta-2\theta_0)}\sin\left[\frac{\theta}{2} - \frac{3\theta_\xi}{2} + \mu\ln\left(\frac{R_0^2}{R_\xi R}\right)\right] \quad \text{for } 0 \le z \le \xi, \tag{14a}$$

$$\varphi_2(x,z,t) = C_2R_\xi^{-3/2}R^{1/2}e^{-\mu(\theta_\xi-\theta)}\sin\left[\frac{\theta}{2} - \frac{3\theta_\xi}{2} + \mu\ln\left(\frac{R_\xi}{R}\right)\right] - C_2R_\xi^{-3/2}R^{1/2}e^{\mu(\theta_\xi+\theta-2\theta_0)}\sin\left[\frac{\theta}{2} - \frac{3\theta_\xi}{2} + \mu\ln\left(\frac{R_0^2}{R_\xi R}\right)\right] \quad \text{for } z > \xi, \tag{14b}$$

where $C_2 = -gq_0a/(2c_pT_0\alpha\mu)$, $R_\xi = (a^2 + D_\xi^2)^{1/2}$, $R_0 = (a^2 + D_0^2)^{1/2}$, $R = (a^2 + D^2)^{1/2}$, $\theta_\xi = \tan^{-1}(-D_\xi/a)$, $\theta_0 = \tan^{-1}(-D_0/a)$, $\theta = \tan^{-1}(-D/a)$, $D_\xi = x - U_\xi t$, $D_0 = x - U_0 t$, and $D = x - Ut$.

The above solution (13) or (14) in each region is the relevant Green's function in the case of the line-type pulse forcing. Therefore, solutions to the finite-depth pulse forcing, line-type steady forcing, and finite-depth steady forcing can be constructed by integrating the Green's function with respect to the level or time or both. Suppose that diabatic forcing is distributed uniformly in the vertical with the forcing bottom and top heights of $d_1$ and $d_2$, respectively. Then, it can be shown that the solution for the perturbation streamfunction in the finite-depth pulse forcing case is expressed by

$$\varphi_1(x,z,t) = \mathrm{Re}\{C_3t^{-1}(BZ)^{1/2+i\mu}[(B2)^{-1/2-i\mu} - (B1)^{-1/2-i\mu}] - C_3t^{-1}(BZ)^{1/2-i\mu}(B0)^{2i\mu} \times [(B2)^{-1/2-i\mu} - (B1)^{-1/2-i\mu}]\} \quad \text{for } 0 \le z \le d_1, \tag{15a}$$

$$\varphi_2(x,z,t) = \mathrm{Re}\{C_3t^{-1}[(BZ)^{1/2+i\mu}(B2)^{-1/2-i\mu} - 1] - C_3t^{-1}(BZ)^{1/2-i\mu}(B0)^{2i\mu}(B2)^{-1/2-i\mu} + C_4t^{-1}[1 - (BZ)^{1/2-i\mu}(B1)^{-1/2+i\mu}] + C_3t^{-1}(BZ)^{1/2-i\mu}(B0)^{2i\mu}(B1)^{-1/2-i\mu}\} \quad \text{for } d_1 < z \le d_2, \tag{15b}$$

$$\varphi_3(x,z,t) = \mathrm{Re}\{C_4t^{-1}(BZ)^{1/2-i\mu}[(B2)^{-1/2+i\mu} - (B1)^{-1/2+i\mu}] - C_3t^{-1}(BZ)^{1/2-i\mu}(B0)^{2i\mu} \times (B2)^{-1/2-i\mu} - (B1)^{1/2-i\mu}]\} \quad \text{for } z > d_2. \tag{15c}$$

Here, $C_3 = C_1/[\alpha(-\mu + i/2)]$, $C_4 = C_1/[\alpha(\mu + i/2)]$, $(B1) = a - i(x - U_1 t)$, and $(B2) = a - i(x - U_2 t)$, where $U_1$ and $U_2$ are the basic-state winds at the bottom and top heights of diabatic forcing, respectively. The solution to the line-type steady forcing, denoted by $f_{l,s}$, can be evaluated using

$$f_{l,s}(x, z, t) = \int_0^t f_{l,p}(x, z, t - \tau)\, d\tau, \tag{16}$$

where $f_{l,p}$ denotes the solution to the line-type pulse forcing. The solution to the finite-depth steady forcing, denoted by $f_{d,s}$, can be evaluated using

$$f_{d,s}(x, z, t) = \int_0^t f_{d,p}(x, z, t - \tau)\, d\tau, \tag{17}$$

where $f_{d,p}$ denotes the solution to the finite-depth pulse forcing. The numerical integrations in (16) and (17) are performed using the Simpson's rule. The perturbation horizontal and vertical velocities can be obtained analytically from (13) [or (14)] and (15) using the relationships of $u = \partial\varphi/\partial z$ and $w = -\partial\varphi/\partial x$.

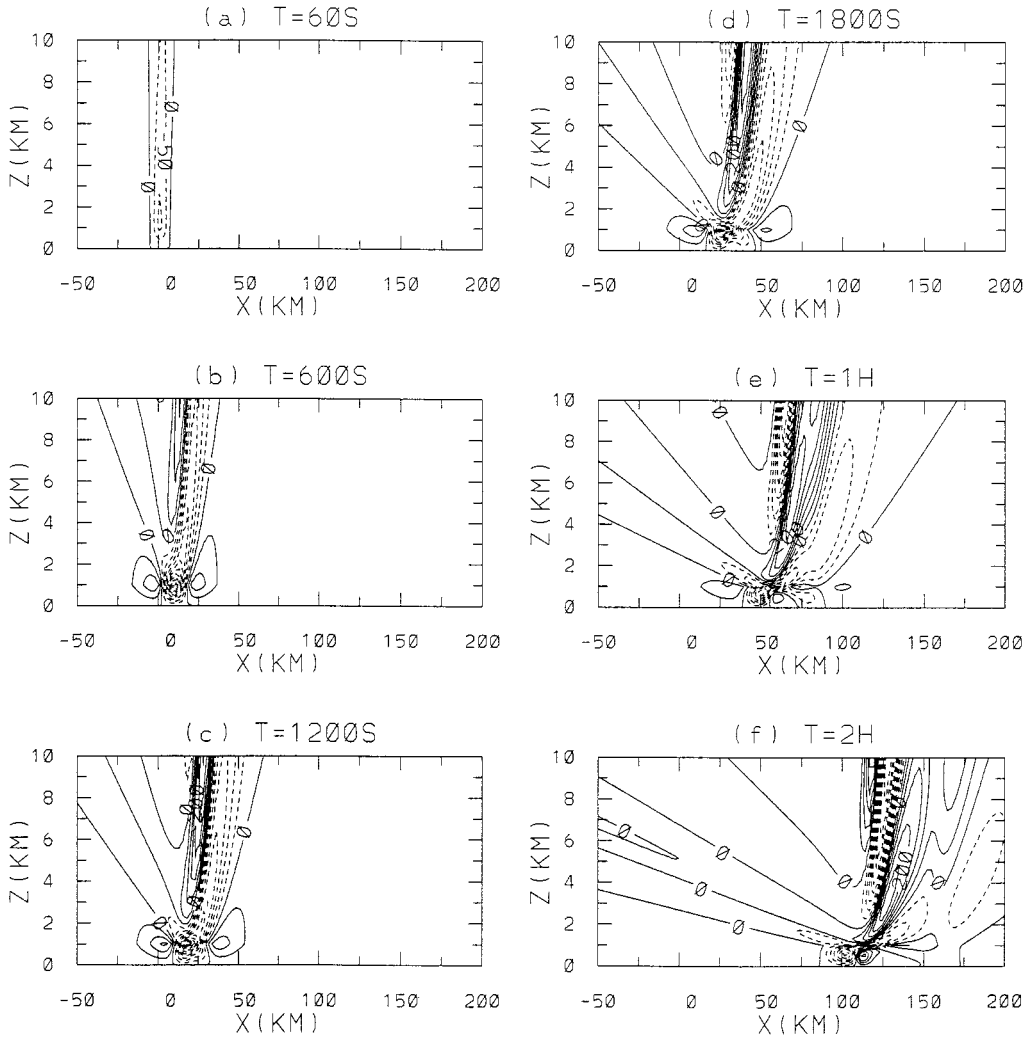


FIG. 1. The time evolution of the perturbation vertical velocity field at the time steps of (a) 60 s, (b) 600 s, (c) 1200 s, (d) 1800 s, (e) 1 h, and (f) 2 h in the line-type pulse cooling case. The critical level is located at $z = 5$ km and the cooling is located at $z = 1$ km. The parameters specified are $N = 0.01$ s$^{-1}$, $T_0 = 273$ K, $a = 10$ km, $U_0 = 20$ m s$^{-1}$, and $q_0 = -3$ J kg$^{-1}$ s$^{-1}$. The values are scaled by $10^9$ and the (actual) contour interval is $5 \times 10^{-8}$ m s$^{-1}$.

## 3. Results and discussion

Figure 1 shows the time evolution of the perturbation vertical velocity fields at the time steps of 60 s, 600 s, 1200 s, 1800 s, 1 h, and 2 h in the line-type pulse cooling case. The parameters considered are $N = 0.01$ s$^{-1}$, $T_0 = 273$ K, and $a = 10$ km. These parameter values are used for all the calculations presented below. The basic-state wind at the surface is specified as $U_0 = 20$ m s$^{-1}$ and the critical level is located at $z = 5$ km. The diabatic cooling with $q_0 = -3$ J kg$^{-1}$ s$^{-1}$ is impulsively applied at $t = 0$ s and at the height of $z = 1$ km. In this setting, the basic-state wind below the critical level blows from left to right and reverses its direction above it, the Richardson number of the basic-state flow ($\mathrm{Ri} = N^2/\alpha^2$) is 6.25, and the diabatic cooling is located below the critical level.

At $t = 60$ s, weak downward motion produced by the initial pulse cooling is dominant in the vertical and its maximum is located near the forcing level ($z = 1$ km). At $t = 600$ s, the initial downdraft intensifies and moves downstream and weak compensating upward motion is observed on both sides of the low-level downdraft. In this study, the terms upstream and downstream are used in reference to the basic-state wind direction where the thermal forcing is applied. Above $z \sim 2$ km, the downdraft with a slight tilt toward the horizontal is followed by updraft. As time goes on, the initially formed downdraft above $z \sim 2$ km continues to move downstream while intensifying and then weakening with a gradual tilt toward the horizontal. Similarly, the updraft located above $z \sim 3$ km behind the downdraft at $t = 600$ s moves downstream while intensifying and

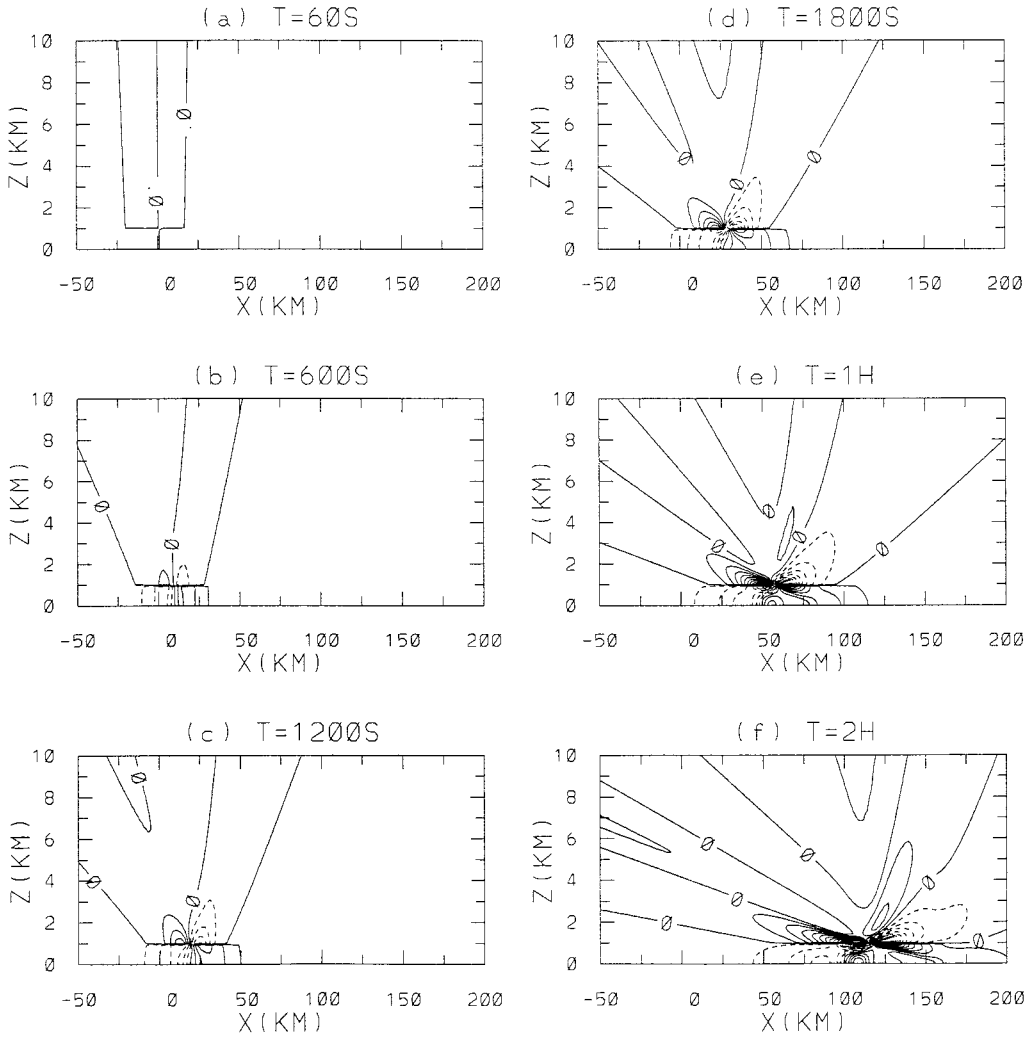


FIG. 2. The same as in Fig. 1 except for the perturbation horizontal velocity field. The contour interval is $1 \times 10^{-6}$ m s$^{-1}$.

then weakening. At $t = 2$ h, its maximum is located at $z \sim 3.5$ km. Weak downdraft observed behind the intensifying updraft at $t = 1200$ s moves downstream and intensifies. At $t = 1$ h, another weak updraft behind this downdraft appears and at $t = 2$ h it intensifies. The low-level downdraft moves downstream. We will call a group of the above-mentioned moving perturbations the ''moving mode.'' From Fig. 1, it is seen that the center of the moving mode travels downstream with a speed of the basic-state wind at the level where the forcing is located, that is, 16 m s$^{-1}$ in this case. This is apparent from the solution for the perturbation vertical velocity, which can be easily derived from (13) using the relationship of $w = -\partial\varphi/\partial x$. This contains terms of the form $[b - i(x - U_\xi t)]^\beta$, where $\beta$ is complex. Also, it is seen that after some time the magnitude of the perturbation vertical velocity at the center of the moving mode remains almost constant. This can be verified by putting $x = U_\xi t$ and $z = \xi$ into the solution for the perturbation vertical velocity.

It is interesting to observe in Fig. 1 that the vertically extended updraft behind the downdraft at $t = 1800$ s has two maxima at $t = 1$ h and appears to split into two updrafts at $t = 2$ h and that the downdraft, which is produced by the initial pulse cooling, at $t = 1$ h appears to split into two downdrafts at $t = 2$ h. A partitioning of the perturbation vertical velocity field into the direct response and the reflected response from the flat bottom indicated that this kind of splitting-like phenomenon shown in Fig. 1 results from a combination of direct gravity waves from the thermal forcing and reflected gravity waves from the bottom.

The time evolution of the perturbation horizontal velocity field corresponding to Fig. 1 is shown in Fig. 2. In response to the initial cooling, there is divergence below the cooling level and convergence above it (e.g.,

at $t = 600$ s). Some patterns observed in the perturbation vertical velocity field (Fig. 1) are similarly observed in the perturbation horizontal velocity field (Fig. 2). For example, the negative perturbation horizontal velocity just above the cooling level at $t = 600$ s strengthens and moves downstream with a gradual horizontal tilt as time goes on. The newly formed positive perturbation horizontal velocity behind this negative perturbation horizontal velocity, clearly observed at $t = 1$ h, strengthens and moves downstream at $t = 2$ h. As in the perturbation vertical velocity, the center of the moving mode travels downstream with a speed of the basic-state wind at the forcing level. However, unlike in the perturbation vertical velocity, after some time the magnitude of the perturbation horizontal velocity at the center of the moving mode continues to increase with time. It can be verified that the perturbation horizontal velocity at the center of the moving mode is proportional to $\sim t$ by putting $x = U_\xi t$ and $z = \xi$ into the solution for the perturbation horizontal velocity, which can be obtained from (13) using the relationship of $u = \partial\varphi/\partial z$. In the corresponding case of the transient response in a uniform basic-state flow (Lin and Smith 1986), the magnitudes of the perturbation vertical and horizontal velocities at the center of the moving mode decrease after some time.

Figures 1 and 2 show that the magnitudes of the perturbations near the region of the line-type pulse cooling after the center of the moving mode travels far downstream, say at $t = 2$ h, are very small compared with those associated with the moving mode. So, it might be deduced that there is no critical-level effect in the case of the line-type pulse forcing. However, as shown below, this is not true. Figure 3 shows the perturbation vertical velocity profiles on the line $x = 0$ km at $t = 5$ h in the line-type pulse cooling case corresponding to Fig. 1. For the moving mode not to significantly affect perturbation behavior near $x = 0$ km line, we allow for a sufficient time lapse so that the center of the moving mode travels far downstream away from $x = 0$ km. Figure 3a, plotted in a linear scale, clearly shows that the perturbation is almost absorbed at the critical level ($z = 5$ km). Figure 3a also shows that the vertical wavelength of gravity waves decreases approaching the critical level because it is proportional to the basic-state wind speed. Immediately after the pulse cooling is applied in a stably stratified atmosphere, internal gravity waves with a spectrum of horizontal phase speeds (group velocities) are generated (note that the horizontal components of the phase velocity and group velocity are equal for the present hydrostatic waves). As time goes on, gravity waves with zero or near-zero horizontal phase speeds stay near $x = 0$ (Bretherton 1988) and experience the critical-level effect. The absolute perturbation vertical velocity profile in Fig. 3b, plotted in a log scale, reveals absorption of the perturbation across the critical level by a factor of $e^{-7} \sim e^{-8}$. This attenuation factor is close to that predicted by linear steady-state

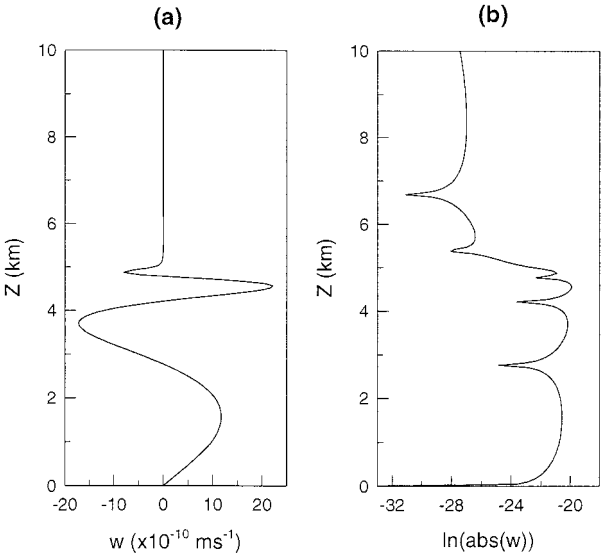


FIG. 3. The perturbation vertical velocity profiles on the line $x = 0$ km at the time step of 5 h in the line-type pulse cooling case corresponding to Fig. 1. The perturbation vertical velocity in (a) is in a linear scale and the perturbation vertical velocity in (b) is in a natural log scale of its absolute value.

studies (Booker and Bretherton 1967; Lin 1987; Lin and Chun 1991; Chun and Lin 1995)—that is, $e^{-\pi\mu}$. Note that in the case of Fig. 3, Ri = 6.25 and $e^{-\pi\mu} = e^{-7.7}$.

In our transient case, the attenuation degree of gravity waves passing through a critical level can be rigorously derived by examining the perturbation streamfunction solution given by (14). Note that the argument below can be equivalently applied to the perturbation vertical velocity. In connection with the linear steady-state studies, consider the solution behavior in the vicinity of $x = 0$ as $t \to \infty$ and denote the critical level by $z_c$. Note that the basic-state wind blows from left to right below the critical level and reverses its direction above it and that the line-type pulse forcing is applied at the level of $z = \xi$. Consider the case in which the thermal forcing is located below a critical level. When $z < z_c$, $D_\xi \to -\infty$, $D_0 \to -\infty$, and $D \to -\infty$, and accordingly $\theta_\xi \to \pi/2$, $\theta_0 \to \pi/2$, and $\theta \to \pi/2$. So, $\exp[-\mu(\theta_\xi - \theta)] \to 1$ and $\exp[\mu(\theta_\xi + \theta - 2\theta_0)] \to 1$. When $z > z_c$, $D_\xi \to -\infty$, $D_0 \to -\infty$, and $D \to \infty$, and accordingly $\theta_\xi \to \pi/2$, $\theta_0 \to \pi/2$, and $\theta \to -\pi/2$. So, $\exp[-\mu(\theta_\xi - \theta)] \to \exp(-\pi\mu)$ and $\exp[\mu(\theta_\xi + \theta - 2\theta_0)] \to \exp(-\pi\mu)$. Now, consider the case in which the thermal forcing is located above a critical level. When $z < z_c$, $D_\xi \to \infty$, $D_0 \to -\infty$, and $D \to -\infty$, and accordingly $\theta_\xi \to -\pi/2$, $\theta_0 \to \pi/2$, and $\theta \to \pi/2$. So, $\exp[\mu(\theta_\xi - \theta)] \to \exp(-\pi\mu)$ and $\exp[\mu(\theta_\xi + \theta - 2\theta_0)] \to \exp(-\pi\mu)$. When $z > z_c$, $D_\xi \to \infty$, $D_0 \to -\infty$, and $D \to \infty$, and accordingly $\theta_\xi \to -\pi/2$, $\theta_0 \to \pi/2$, and $\theta \to -\pi/2$. So, $\exp[-\mu(\theta_\xi - \theta)] \to 1$ and $\exp[\mu(\theta_\xi + \theta - 2\theta_0)] \to \exp(-2\pi\mu)$. The attenuation factor $\exp(-2\pi\mu)$ results from the fact that gravity waves pass through the critical level twice. That is, gravity waves propagate downward

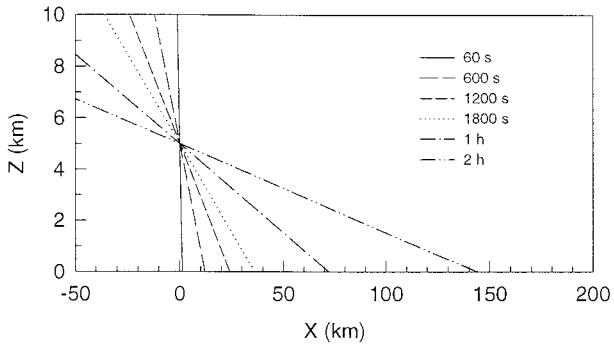


FIG. 4. The lines of transient critical levels at different time steps in the line-type pulse cooling case corresponding to Fig. 1.

across the critical level, they are totally reflected from the bottom, and the reflected waves propagate upward again across the critical level. Therefore, (14) clearly indicates that gravity waves are attenuated by a factor of $\exp(-\pi\mu)$ whenever passing through a critical level. This result suggests that in a limit our transient critical-level solution includes previous steady-state critical-level solution (Lin 1987; Lin and Chun 1991).

Next, the transient critical-level effect is examined. For the basic-state wind considered in this study, the transient critical level for internal gravity waves originated at $x = 0$ is given by

$$z_{ct} = \frac{1}{\alpha}\left(U_0 - \frac{x}{t}\right). \tag{18}$$

For $t \to \infty$, $z_{ct}$ approaches to $U_0/\alpha$, which is the prescribed critical level. The tilt of critical level with respect to the horizontal line decreases with time. This is seen in Fig. 4, which shows the lines of transient critical levels for gravity waves originated at $x = 0$ at different time steps in the line-type pulse cooling case. When the critical level is located above (below) the forcing level ($z = 1$ km) for a certain location and time, the amplitude of waves above (below) the critical level becomes small by the critical-level attenuation.

Figure 5 shows the absolute perturbation vertical velocity profiles in a log scale on the lines $x = 80$ km and 130 km at the time step of 2 h in the line-type pulse cooling case corresponding to Fig. 1f. At this time, the center of the moving mode is located at $x = 115.2$ km. The transient critical levels at $x = 80$ km and 130 km at $t = 2$ h are located at $z = 2.22$ km and 0.49 km, respectively. That is, the critical level is located above the forcing level at $x = 80$ km, whereas it is located below the forcing level at $x = 130$ km. The perturbation vertical velocity at $x = 80$ km shows an abrupt decrease in its magnitude across $z \sim 2.2$ km by the critical-level attenuation. The magnitude of the perturbation vertical velocity at $x = 130$ km decreases below $z \sim 0.5$ km by the critical-level attenuation. The degree of attenuation of transient waves across the critical level is closer to $\exp(-\pi\mu)$ as going farther away from the center of the moving mode. The above-mentioned transient critical-level effect explains in Fig. 1 why the magnitude of the perturbation vertical velocity above the critical level to the right of the vertical line passing through the center of the moving mode is much larger than that to the left of the line.

To investigate transient flow behavior near the pulse cooling origin and moving mode and compare results with previous studies, the vertical displacement $\eta$ for the line-type pulse forcing is evaluated from the perturbation vertical velocity using the relationship of $w = d\eta/dt$:

$$\begin{aligned}\eta_1(x,z,t) &= -C_2 t R_\xi^{-3/2} R^{-1/2} e^{\mu(\theta_\xi-\theta)} \cos\left[\frac{\theta}{2}+\frac{3\theta_\xi}{2}+\mu\ln\left(\frac{R_\xi}{R}\right)\right] \\ &\quad + C_2 t R_\xi^{-3/2} R^{-1/2} e^{\mu(\theta_\xi+\theta-2\theta_0)} \\ &\quad \times \cos\left[\frac{\theta}{2}+\frac{3\theta_\xi}{2}-\mu\ln\left(\frac{R_0^2}{R_\xi R}\right)\right] \quad \text{for } 0 \le z \le \xi, \end{aligned} \tag{19a}$$

$$\begin{aligned}\eta_2(x,z,t) &= -C_2 t R_\xi^{-3/2} R^{-1/2} e^{-\mu(\theta_\xi-\theta)} \cos\left[\frac{\theta}{2}+\frac{3\theta_\xi}{2}-\mu\ln\left(\frac{R_\xi}{R}\right)\right] \\ &\quad + C_2 t R_\xi^{-3/2} R^{-1/2} e^{\mu(\theta_\xi+\theta-2\theta_0)} \\ &\quad \times \cos\left[\frac{\theta}{2}+\frac{3\theta_\xi}{2}-\mu\ln\left(\frac{R_0^2}{R_\xi R}\right)\right] \quad \text{for } z > \xi. \end{aligned} \tag{19b}$$

Figure 6a shows the time series of the vertical displacement at the location of $x = 0$ km and $z = 1$ km, and Fig. 6b shows the vertical displacement at different time steps at $z = 1$ km in a moving frame with the basic-state wind. At the pulse cooling origin, the displacement at very early times is downward. As the compensating updraft on the left side of the initially formed downdraft in response to the cooling moves downstream (see Fig. 1), the displacement gradually changes from downward to upward. The maximum upward displacement occurs at about $t = 1200$ s. As the moving disturbance moves further downstream, the upward displacement becomes diminished. The observed negative phase relationship between the cooling and the induced vertical displacement near the cooling source region after some time is consistent with previous steady-state (Smith and Lin 1982) and transient (Lin and Smith 1986) studies. The decay rate of the vertical displacement in Fig. 6a can be easily determined by examining (19) at $x = 0$ and $z = \xi$; that is,

$$\begin{aligned}\eta(0,\xi,t) &= -C_2 t R_\xi^{-2} \cos(2\theta_\xi) + C_2 t R_\xi^{-2} e^{2\mu(\theta_\xi-\theta_0)} \\ &\quad \times \cos\left[2\theta_\xi - \mu\ln\left(\frac{R_0^2}{R_\xi^2}\right)\right]. \end{aligned} \tag{20}$$

The above equation indicates that after some time the

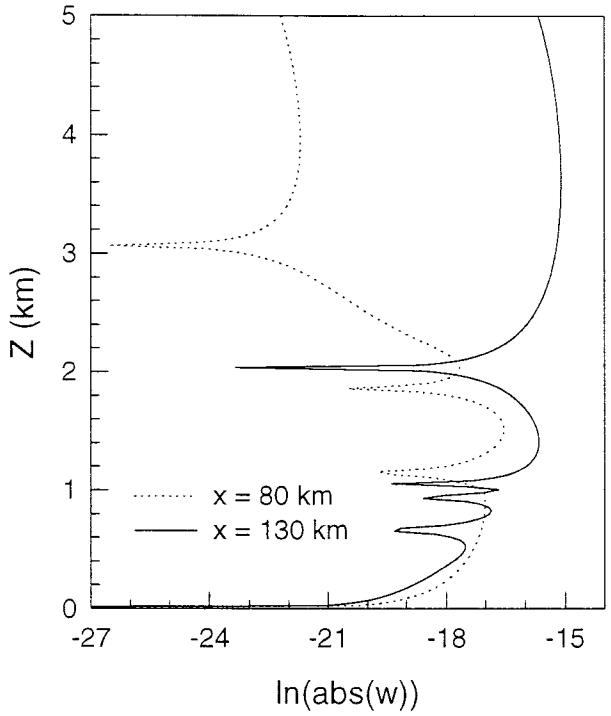


FIG. 5. The absolute perturbation vertical velocity profiles on the lines $x = 80$ km (dotted line) and 130 km (solid line) at the time step of 2 h in the line-type pulse cooling case corresponding to Fig. 1f. The perturbation vertical velocity is in a natural log scale of its absolute value.

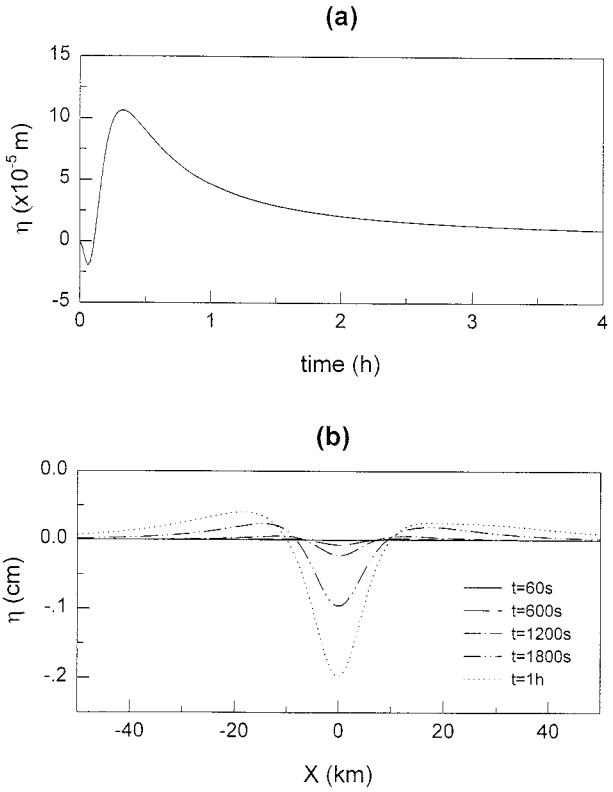


FIG. 6. (a) The time series of the vertical displacement at the location of $x = 0$ km and $z = 1$ km and (b) the vertical displacement at the time steps of 60 s, 600 s, 1200 s, 1800 s, and 1 h at the level of $z = 1$ km in a frame moving with a speed of the moving mode at $z = 1$ km. Both figures are for the line-type pulse cooling case corresponding to Fig. 1.

vertical displacement decays as $t^{-1}$ because $R_{\xi}^{-2}$ decays as $t^{-2}$. This decay rate of the vertical displacement was also found in the uniform basic-state wind case (Lin and Smith 1986). Using group velocity arguments, Bretherton (1988) showed that the $t^{-1}$ decay of the vertical displacement is a geometric consequence of wave dispersion in two dimensions.

Figure 6b shows that near the center of the moving mode there exists downward displacement with weak upward displacements on both sides of the growing disturbance. By putting $x = U_{\xi}t$ and $z = \xi$ into (19), after some time the vertical displacement at the center of the moving mode can be shown to grow as $\sim t$. This result is different from that of the transient response in a uniform flow, which shows that the vertical displacement at the center of the moving mode remains constant after some time (Lin and Smith 1986). This figure also shows that the vertical displacement is not exactly symmetric about the central axis of the moving mode. This is due to the wave reflection from the bottom. The upward displacement to the upstream of the growing disturbance is slightly larger than that to the downstream.

Next, consider the case in which the finite-depth cooling is impulsively applied at $t = 0$ s. Figure 7 shows the time evolution of the perturbation vertical velocity field at different time steps in the finite-depth pulse cooling case. The pulse cooling is specified uniformly in the vertical from the surface to $z = 1.5$ km. Compared with the line-type pulse cooling case (Fig. 1), there are some similarities in that the center of the moving mode travels downstream with a basic-state wind speed and that updraft and downdraft experience processes of formation, intensification, and weakening while moving downstream. On the other hand, there are some differences in that after some time the magnitude of the perturbation vertical velocity at the line that connects the centers of the moving modes at the forcing top and bottom decreases with time ($\sim t^{-1}$) and that the centers of the moving modes become separated and distant. These similarities and differences can be easily understood by regarding the response to the finite-depth pulse cooling as a sum of an infinite number of responses to line-type pulse coolings.

Denote the horizontal distance between the center of the moving mode at the cooling bottom level ($z = 0$ km) and the center of the moving mode at the cooling top ($z = 1.5$ km) by $d_m$. Since each moving mode corresponding to individual line-type pulse cooling travels downstream with a basic-state wind speed at the cooling level, the distance is given by $d_m = [U(z = 0 \text{ km}) - U(z = 1.5 \text{ km})]t = (20 - 14)t = 6t$. Thus, the distance

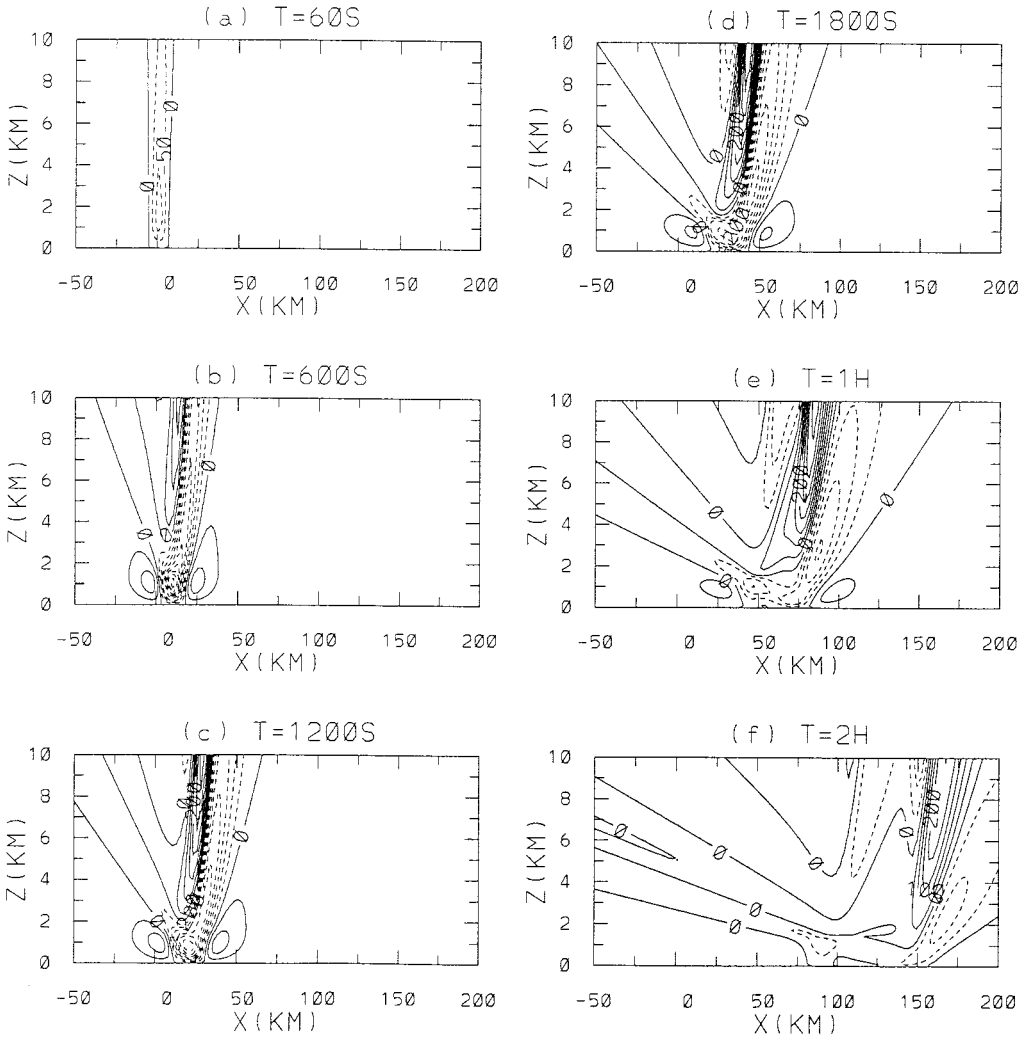


FIG. 7. The same as in Fig. 1 except for the finite-depth pulse cooling case. The pulse cooling is specified uniformly in the vertical from the surface to $z = 1.5$ km. The contour interval is $5 \times 10^{-5}$ m s$^{-1}$.

$d_m$ linearly increases with time. At early times, the pattern of the perturbation vertical velocity field in the finite-depth pulse cooling case (Figs. 7a, 7b, and 7c) is very similar to that in the line-type pulse cooling case (Figs. 1a, 1b, and 1c) because $d_m$ is very small (e.g., $d_m = 7.2$ km at $t = 1200$ s) compared with the horizontal plotting domain size of 250 km. However, at early times the magnitude of the perturbation vertical velocity in the finite-depth pulse cooling case is much larger than that in the line-type pulse cooling case. This is because perturbations in responses to individual line-type pulse cooling are almost in phase with each other within a short distance and hence work constructively to yield larger perturbation. As time goes on, the moving modes near the cooling bottom and top levels are clearly observed and their centers gradually become distant (see Figs. 7e and 7f). After some time, the magnitude of the perturbation vertical velocity at the line that connects the center of the moving mode at the forcing top and that at the forcing bottom decreases with time because of the geometric expansion of the line. Further analysis indicated that near the finite-depth pulse cooling region the critical-level absorption is clearly observed.

So far, the cases in which the thermal forcing was impulsively applied to a stably stratified atmosphere in the presence of a critical level have been examined. Next, the cases in which the thermal forcing is steadily applied to the atmosphere will be investigated. Figure 8 shows the time evolution of the perturbation vertical velocity field in the line-type steady cooling case. The line-type cooling is located at $z = 1$ km and steadily applied starting from $t = 0$ s. The pattern in the early response fields at $t = 60$ s and 600 s is similar to that in the pulse cooling cases (Figs. 1 and 7), but as time goes on further, in addition to the moving mode, there appears to be another kind of mode near the steady

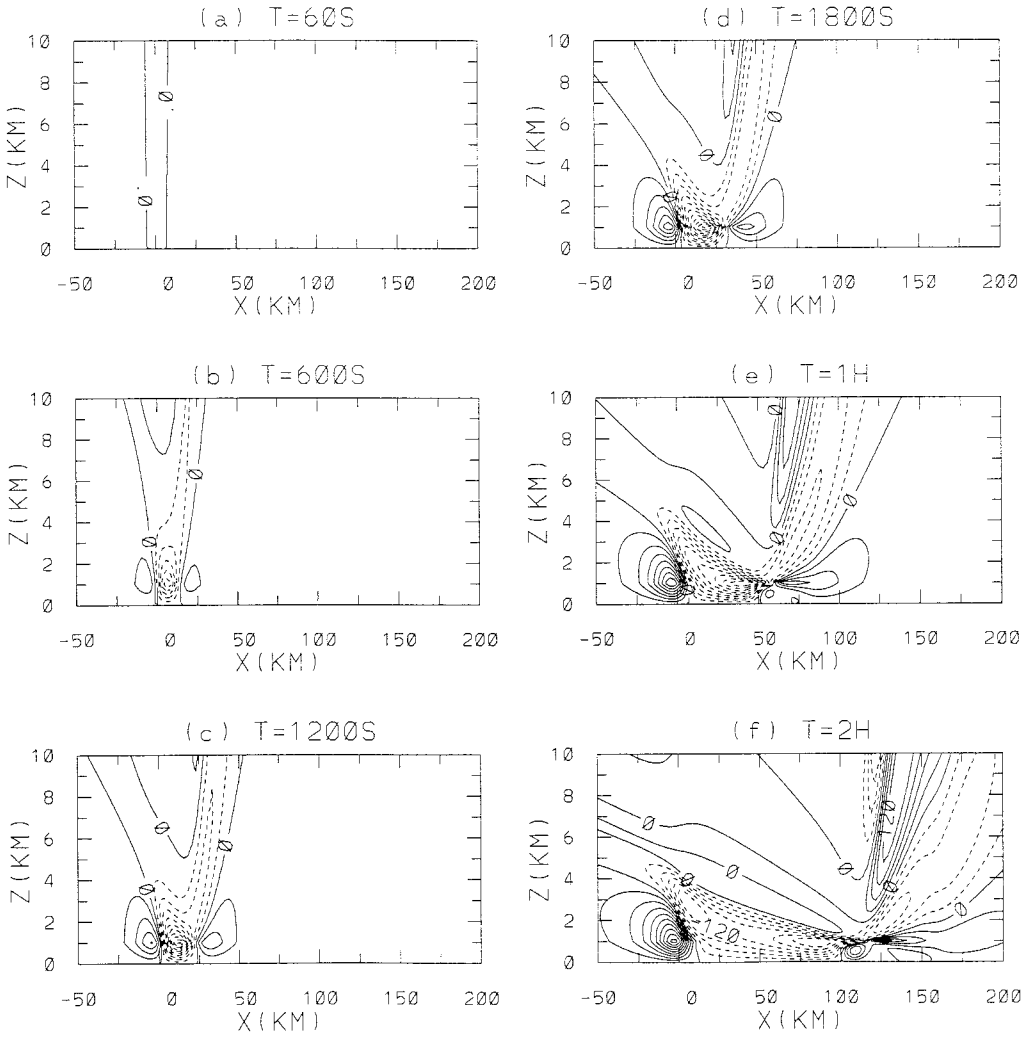


FIG. 8. The same as in Fig. 1 except for the line-type steady cooling case. The line-type cooling is steadily applied starting from $t = 0$ s. The contour interval is $3 \times 10^{-5}$ m s$^{-1}$.

cooling region. We will call a group of the perturbations that develop and stay near the steady forcing region the ''stationary mode.'' As time goes on, the moving mode and stationary mode become distant and distinctive (see the fields at $t = 1800$ s, 1 h, and 2 h). The perturbation pattern above the cooling level in the vicinity of the moving mode with time appears to be similar to that in the line-type pulse cooling case (Fig. 1). The noticeable moving mode is produced at very early times and then travels downstream with a speed of the basic-state wind at the cooling level. The magnitude of this moving mode is much larger than that in the line-type pulse cooling case because the cooling is steady (cf. Fig. 8 with Fig. 1). The response to the line-type steady cooling can be regarded as a sum of an infinite number of responses to line-type pulse coolings, which are continuously added in time to the flow system. Therefore, a group of perturbations that are produced at very early times and move farthest downstream retain identity explicitly in the moving mode. However, perturbations that are produced after the beginning and move downstream are destructively combined to yield very small magnitudes because of different phases of responses to individual line-type pulse cooling released at different times.

Figure 8 shows that the magnitude of the perturbation vertical velocity in the stationary mode gradually increases with time. This is because perturbations induced by individual line-type cooling with zero or near-zero horizontal phase speeds, although very small in magnitude, are constructively combined near the cooling region to result in large magnitudes. At $t = 2$ h, the maximum magnitude of the perturbation vertical velocity in the stationary mode is even larger than that in the moving mode. It is also clear that the stationary mode experiences the critical-level effect. After the moving mode moves downstream far away from the stationary mode, the upward motion is present near the cooling region. The phase relationship between the cooling and

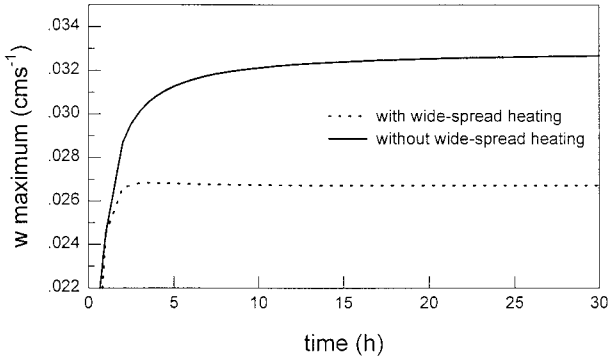


FIG. 9. The time series of the maximum perturbation vertical velocity associated with the stationary mode with and without a widespread heating term in the line-type steady cooling case corresponding to Fig. 8. In the case of including a widespread heating term, the parameter $a_1$ is set to 5a.

the induced vertical velocity near the forcing region is negative, consistent with previous studies (e.g., Smith and Lin 1982). Figure 8 confirms that the negative phase relationship is directly related to the steadiness (Lin and Smith 1986). In the stationary mode, the phase is tilted upstream, implying upward energy propagation. Note in Fig. 8 that due to the moving mode, the region of downward motion near the surface spreads over a large area.

In a two-dimensional, linear, steady-state, inviscid flow system, a widespread cooling (heating) term is needed to avoid a net heating (cooling) problem (Smith and Lin 1982). To examine the effect of including a widespread heating term on the transient flow response, the time series of the maximum perturbation vertical velocity associated with the stationary mode is plotted in Fig. 9. The horizontal structure of thermal forcing is specified as

$$f(x) = \frac{a^2}{x^2 + a^2} - \frac{aa_1}{x^2 + a_1^2}, \tag{21}$$

where $a_1$ is a constant with $a_1 > a$. The parameter $a_1$ is set to $5a$ ($a = 10$ km). Note in (21) that the net cooling at any level is zero. When the widespread heating term is not added, the maximum perturbation vertical velocity associated with the stationary mode continues to increase with time, although the rate of increase after a long time becomes very small. On the other hand, when the widespread heating term is added, the maximum perturbation vertical velocity virtually reaches a steady state after $t \sim 3$ h. These results indicate that in the transient case with two dimensions the widespread heating (cooling) term is also needed to get a steady-state response field in the stationary mode.

It is expected from the previous results (Figs. 7 and 8) that in response to finite-depth steady cooling there will be two kinds of response characteristics: the separation of the moving mode observed in response to the finite-depth pulse cooling, and the stationary mode observed in response to the line-type steady cooling. Figure 10 shows the time evolution of the perturbation vertical velocity field in the finite-depth steady cooling case. The cooling is specified uniformly in the vertical from the surface to $z = 1.5$ km and is steadily applied starting from $t = 0$ s. The expected characteristics are observed in Fig. 10. The magnitude of the perturbation vertical velocity in the moving mode is relatively small compared with that in the stationary mode. This is because the horizontal area occupied by moving modes that are individually originated at different cooling levels becomes large with time, whereas the perturbations in the stationary mode occupy a certain horizontal extent with time.

Gravity waves play an important role in the transport of momentum and energy from one region to another and a vertical convergence/divergence of the momentum flux influences flow field. To examine a transient behavior of the momentum flux, the vertical profiles of the momentum flux (vertical flux of integrated horizontal momentum) at four different time steps are plotted in Fig. 11. A large horizontal domain size, 800 km from $x = -200$ to 600 km, is chosen to calculate the momentum flux. Because the total energy provided by the cooling increases with time, the momentum flux also increases with time. The momentum flux at the surface is zero because the perturbation vertical velocity is zero there. From the surface to the cooling top ($z = 1.5$ km), the magnitude of the momentum flux increases with height, then decreases to a small value at the critical level, and above it becomes constant. This result is different from that in the steady-state case (Lin 1987) in two regions.

The first region is from the cooling top to the critical level. The theoretical argument (Eliassen and Palm 1960) and analysis in the steady-state case indicate that in the region of no thermal forcing the momentum flux is constant with height. However, our transient study indicates a gradual decrease from the thermal forcing top to the critical level. The transient study with a uniform basic-state wind (Lin and Smith 1986) shows similar behavior. From (1)–(4), one can derive, in the absence of thermal forcing, the vertical gradient of the momentum flux ($U \neq 0$):

$$\frac{\partial}{\partial z}(\overline{uw}) = \frac{1}{N^2 U}\frac{\partial}{\partial t}\left(\frac{\overline{b^2}}{2}\right) - \frac{1}{U_z}\frac{\partial}{\partial z}\frac{\partial}{\partial t}\left(\frac{\overline{u^2}}{2}\right) - \frac{1}{UU_z}\frac{\partial}{\partial z}\left(\overline{\frac{\partial u}{\partial t}\pi}\right), \tag{22}$$

where $U_z = dU/dz$ and any quantity with overbar means a horizontally integrated one. The above equation indicates that in a steady-state case a vertical gradient of the momentum flux is zero, but in a transient case the time variation of the perturbation horizontal velocity and perturbation buoyancy can cause the momentum flux to vary with height. The second region is one above the critical level. The gravity wave response field produced by a pulse forcing in a uniform basic-state wind is sym-

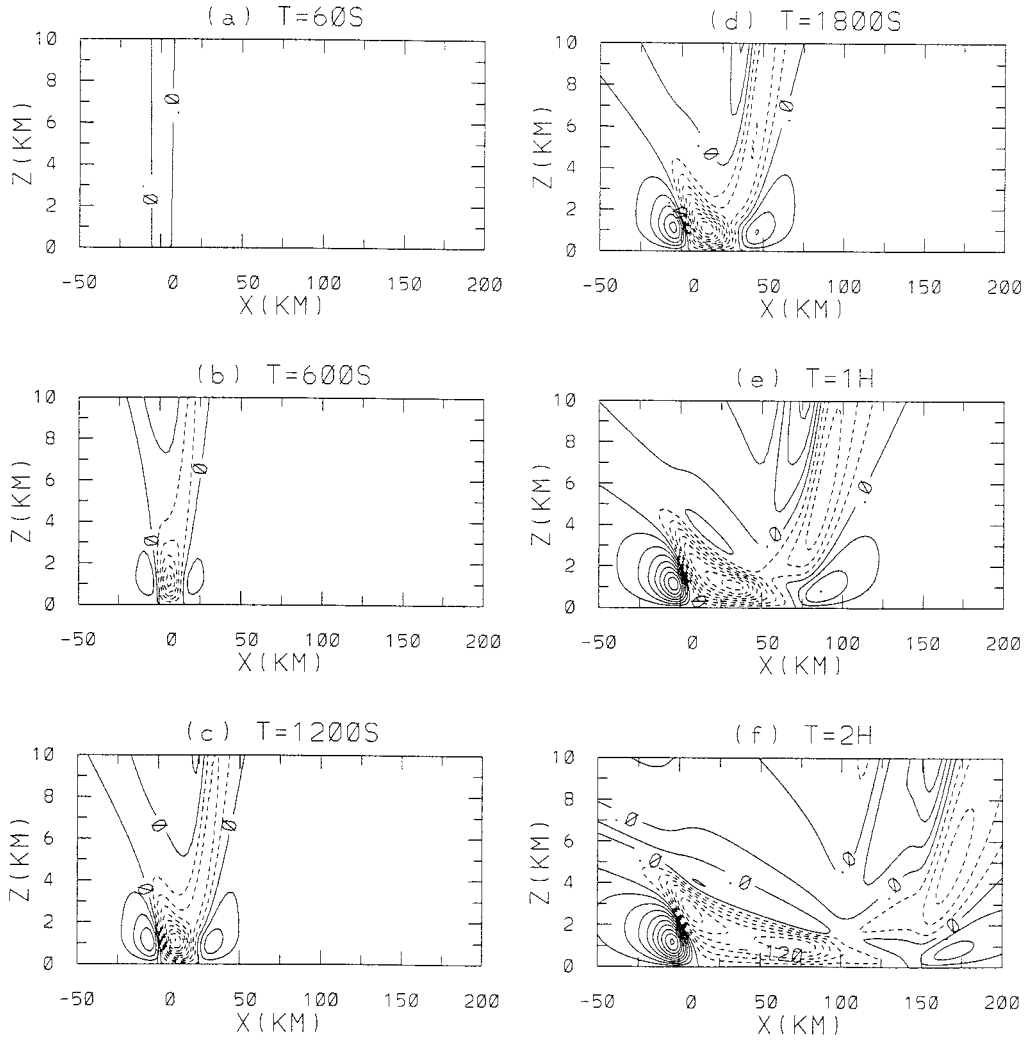


FIG. 10. The same as in Fig. 1 except for the finite-depth steady cooling case. The cooling is specified uniformly in the vertical from the surface to $z = 1.5$ km and is steadily applied starting from $t = 0$ s. The contour interval is $3 \times 10^{-2}$ m s$^{-1}$.

metric about a moving center and in this case gravity waves cannot impart net momentum flux to the flow (Lin 1994). However, the moving mode produced in a sheared flow is not symmetric and gravity waves can impart net momentum flux to the flow. This explains the momentum flux above the critical level in Fig. 11. The positive momentum flux above the critical level implies an upward flux of wave energy since the basic-state wind is negative there.

Now, consider a case in which thermal forcing is located across a critical level. Figure 12 shows the time evolution of the perturbation vertical velocity field in the finite-depth steady heating case. The heating extends uniformly in the vertical from $z = 1$ to 9 km and is steadily applied starting from $t = 0$ s. This heating represents latent heating due to deep cumulus convection. The critical level is located at $z = 5$ km—that is, at the midlevel of the heating. The parameters specified are the same as in Fig. 1 except for $q_0 = 2$ J kg$^{-1}$ s$^{-1}$. Figure 12 indicates that the thermal forcing across the critical level significantly influences flow field. Near the forcing region, the response to the heating located across the critical level shows upward motion at all times. The initial response is weak upward motion extending in the vertical near the heating region (at $t = 60$ s). At $t = 600$ s, the upward motion across the critical level intensifies and compensating downward motion on both sides of the upward motion exists. As time goes on, this updraft region extending over the heating region stays in the vicinity of $x \sim 0$ km, but the compensating downdraft regions move outward (at $t = 1200$ s and 1800 s). At $t = 2$ h, there clearly appear two maxima in the perturbation vertical velocity, which are located near $z = 3.4$ km and 6.2 km. In the steady-state case with the heating in the vicinity of the critical level, two maxima in the vertical velocity are also observed when the Rich-

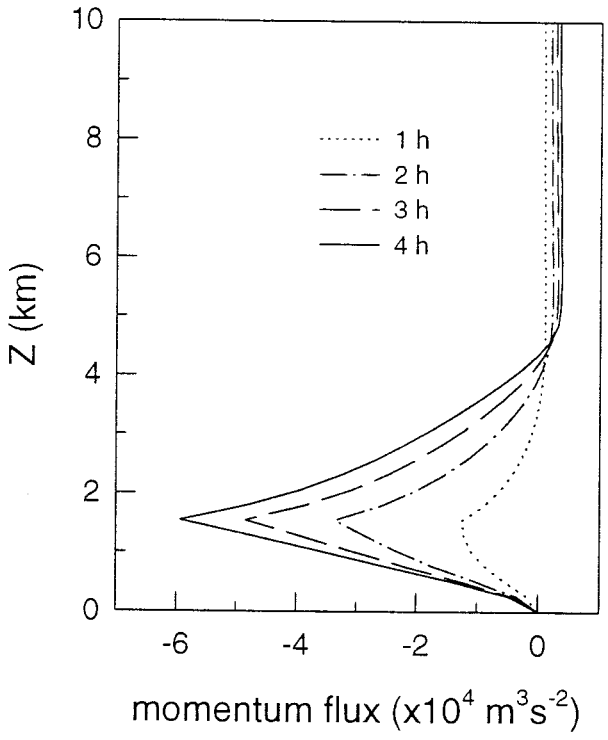


FIG. 11. The vertical profiles of the momentum flux at the time steps of 1 h, 2 h, 3 h, and 4 h in the finite-depth steady cooling case corresponding to Fig. 10.

ardson number of the basic-state flow (Ri) is 5, but in the case of Ri = 1 the maximum vertical velocity is located right at the critical level (Lin 1987). Note that in our case Ri = 6.25. Above the top of the steady heating, the phase of the perturbation vertical velocity is tilted upstream, implying upward propagation of wave energy.

The response to steady thermal forcing located across a critical level can be regarded as a sum of the response to steady thermal forcing extended from the forcing bottom to the critical level and the response to steady thermal forcing extended from the critical level to the forcing top. In response to the steady forcing extended from the forcing bottom to the critical level, it can be easily deduced from Fig. 10, which shows a case of the finite-depth steady cooling below the critical level, that in addition to the stationary mode, the moving mode will move downstream (from left to right). This signal of the moving mode can be seen in the upper-right region of Figs. 12c and 12d (at $t = 1200$ s and 1800 s). Similarly, in response to the steady forcing extended from the critical level to the forcing top, in addition to the stationary mode, the moving mode is expected to move downstream (from right to left). This signal of the moving mode can be seen in the middle-left region (around $x \sim -60$ km and $z \sim 10$ km) of Fig. 12e (at $t = 1$ h), although it is very weak compared with the rightward-moving mode.

The analysis of the perturbation streamfunction (14) and Fig. 3 suggested that our transient critical-level solution includes previous steady-state critical-level solution. To further examine whether our transient solution can include steady-state solution as $t \to \infty$, two cases are considered to compare with previous steady-state studies. The first case is that of finite-depth steady cooling, which is located below a critical level. A widespread heating term is added to obtain transient solution because it is needed to get the solution in a steady-state study. Figure 13a shows the perturbation vertical velocity field calculated from the steady-state solution in the presence of a critical level by Lin (1987). Figure 13b shows the perturbation vertical velocity field at $t = 30$ h calculated from our transient solution. All the parameters specified are the same for both perturbation vertical velocity fields. Although there are minor differences in the region above the critical level where perturbations are very small, the two fields are virtually the same, especially in the region below the critical level. Allowing for some numerical approximation in computing the perturbation vertical velocity at large time, it is certain that after a sufficient time our transient stationary-mode solution in the finite-depth steady forcing case in the presence of a critical level is the steady-state solution of Lin (1987).

The second case is that of finite-depth steady cooling in a uniform basic-state wind. Figure 14a shows the perturbation vertical velocity field calculated from the steady-state solution for a uniform basic-state wind (e.g., Chun and Baik 1994). Figure 14b shows the perturbation vertical velocity field at $t = 30$ h calculated from our transient solution. To compute the perturbation vertical velocity field from the transient solution corresponding to a uniform basic-state wind case, the critical level is located far away from the surface in our transient solution. This is equivalent to a uniform basic-state wind limit of our transient solution in the presence of a critical level. For a computational purpose, the Richardson number of the basic-state flow is set to $8 \times 10^5$ (with $N = 0.01$ s$^{-1}$ and $U_0 = 10$ m s$^{-1}$, the critical level is located at $z \sim 894$ km). A difference in the basic-state wind speed between $z = 0$ km and $z = 10$ km is 0.11 m s$^{-1}$ so the basic-state wind in Fig. 14b can be considered as uniform. The magnitude and pattern of the perturbation vertical velocity in our transient case are virtually the same as those in the steady-state case. It is certain that after a sufficient time a limit to our transient stationary-mode solution produces the steady-state solution in a uniform basic-state wind case. Figures 13 and 14 clearly show that our transient solution indeed includes previous steady-state solutions either in a uniform or a critical-level case. This proves that our solution is quite general. Finally, note that replacing cooling (heating) by heating (cooling) in our transient solution changes only the sign of perturbation because the flow system considered in this study is linear.

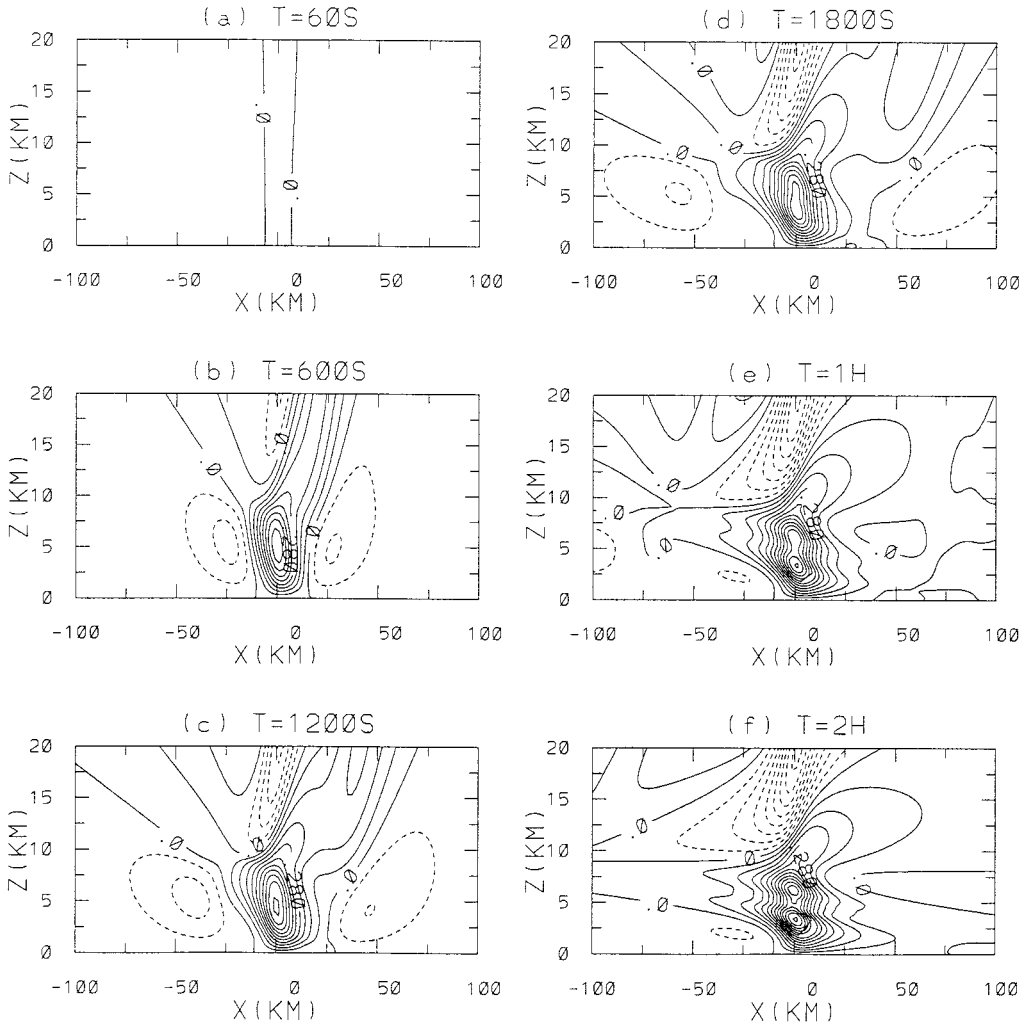


FIG. 12. The time evolution of the perturbation vertical velocity field at the time steps of (a) 60 s, (b) 600 s, (c) 1200 s, (d) 1800 s, (e) 1 h, and (f) 2 h in the finite-depth steady heating case. The heating is specified uniformly in the vertical from $z = 1$ km to 9 km and steadily applied starting from $t = 0$ s. The critical level is located at $z = 5$ km. Other parameters specified are the same as in Fig. 1 except for $q_0 = 2$ J kg$^{-1}$ s$^{-1}$. The contour interval is 0.07 m s$^{-1}$.

## 4. Summary and conclusions

To further understand the dynamics of thermally induced mesoscale circulation, we extended previous studies of the response of an atmosphere to diabatic heating or cooling by including both a time dependency and a critical level. The airflow system considered is a two-dimensional, linearized, hydrostatic, nonrotating, inviscid, Boussinesq system. Under such a simplified flow system, the transient response of a stably stratified atmosphere to thermal forcing in the presence of a critical level was investigated analytically using the Green's function method. The specified thermal forcing is located below or across a critical level. The target solution is for the finite-depth steady forcing, but intermediate solutions to the line-type pulse forcing, finite-depth pulse forcing, and line-type steady forcing are analyzed in detail because these solutions provide some insight into the basic dynamics of the response to the finite-depth steady forcing.

The responses to the pulse forcings showed that the center of the moving mode travels downstream with a speed of the basic-state wind at the level where the thermal forcing is located. In the vicinity of the initial forcing, there clearly exists the gravity wave absorption phenomenon across the critical level, although the relative magnitude of perturbation is very small. This supports the existence of a group of waves with zero or near-zero horizontal phase velocities. In response to the line-type pulse forcing, after some time the magnitude of the perturbation vertical velocity at the center of the moving mode remains almost unchanged with time, whereas the magnitude of the perturbation horizontal

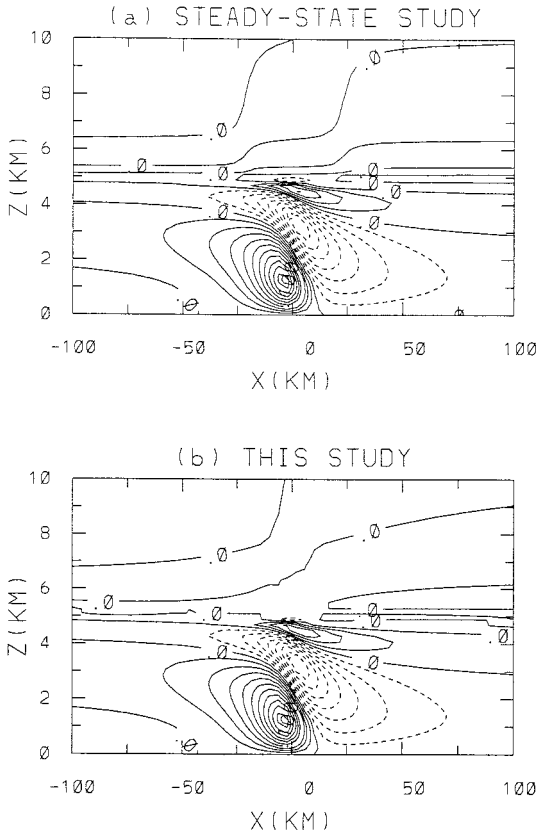


FIG. 13. (a) The perturbation vertical velocity field in the steady-state study of Lin (1987) and (b) that at $t = 30$ h in our finite-depth steady cooling case. The cooling is specified uniformly in the vertical from the surface to $z = 1.5$ km. The critical level is located at $z = 5$ km. In both cases, a widespread heating term is included with $a_1 = 5a$ [see (21)]. Other parameters specified are the same as in Fig. 1. The contour interval is 0.025 m s$^{-1}$.

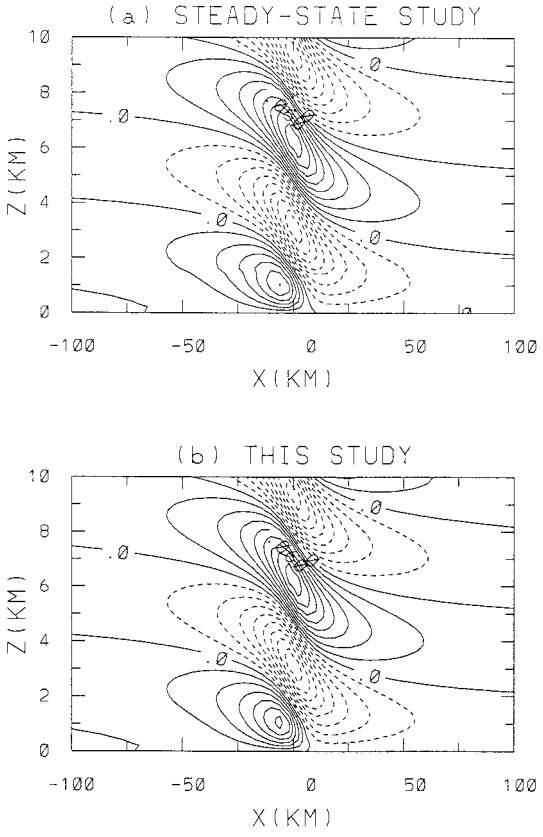


FIG. 14. (a) The perturbation vertical velocity field in the steady-state, uniform basic-state wind case of Chun and Baik (1994) and (b) that at $t = 30$ h in our finite-depth steady cooling case. The cooling is specified uniformly in the vertical from the surface to $z = 1.5$ km. In both cases, a widespread heating term is included with $a_1 = 5a$ [see (21)]. In (a) the basic-state wind is 10 m s$^{-1}$ and in (b) $U_0 = 10$ m s$^{-1}$ and Ri $= 8 \times 10^5$. The $q_0$ is specified as $-0.5$ J kg$^{-1}$ s$^{-1}$. Other parameters specified are the same as in Fig. 1. The contour interval is 0.015 m s$^{-1}$.

velocity at the center of the moving mode increases with time. The transient critical level is a function of the horizontal location and time. In response to the finite-depth pulse forcing, after some time the magnitude of the perturbation vertical velocity at the line that connects the centers of the moving modes at the forcing top and bottom decreases with time. This is due to the geometric expansion of the line.

In responses to the steady forcings, the stationary mode as well as the moving mode appear. The origin of the stationary mode is very small-amplitude waves with zero or near-zero horizontal phase velocities in the pulse forcings. These waves accumulate to be perceptible in responses to the steady forcings. The stationary mode is almost entirely absorbed at the critical level. The dynamics of the moving mode in the steady forcing cases are similar to those in the corresponding pulse forcing cases.

In previous steady-state studies, a widespread heating (cooling) term was included to avoid a net cooling (heating) problem in a two-dimensional, linear, steady-state, inviscid flow system. It was shown that adding a widespread heating (cooling) term eventually results in a steady state in the stationary mode, but without this term the perturbation continues to grow with time. When a widespread heating (cooling) term is added, the eventual response in the stationary mode is virtually the same as the response shown in previous steady-state studies. This proves the generality of our transient solution.

Unlike the steady-state case, the momentum flux was shown to vary with height in the region of no thermal forcing because of the time variation of the perturbation horizontal velocity and perturbation buoyancy. There is a gradual decrease of the momentum flux from the thermal forcing top to the critical level. It was also shown that the moving mode in the present case can transport a small amount of the momentum flux above the critical level.

In this study, the basic dynamics of gravity waves was emphasized, but the solution can be applied to various mesoscale phenomena by constructing realistic

thermal forcing and wind shear appropriate for the particular phenomenon investigated. For example, deep slanting heating across the critical level combined with low-level cooling (Pandya and Durran 1996) can be constructed to explain some aspects of the squall line circulation. In this study, the flow system was restricted to two dimensions. An analytical study of the effects of including a third dimension on the response of a stably stratified atmosphere to thermal forcing is under investigation. In this study, the flow system was also restricted to being linear. Nonlinearity becomes important, for example, as the magnitude of diabatic forcing increases or the basic-state wind decreases. The nonlinear flow response to thermal forcing might be quite different from the linear flow response depending on the inverse Froude number associated with thermally induced waves and the degree of nonlinearity. A systematic study of flow regimes in the nonlinear response of a stably stratified atmosphere to thermal forcing is needed to further enhance our understanding of thermally induced mesoscale circulation.

*Acknowledgments.* The authors would like to thank three anonymous reviewers for providing valuable comments on this study. The authors acknowledge the Korea Systems Engineering Research Institute for providing a computing environment on the CRAY C90 for this research.

## REFERENCES

Angell, J. K., D. H. Pack, C. R. Dickson, and W. H. Hoecker, 1971: Urban influence on nighttime airflow estimated from tetroon flights. *J. Appl. Meteor.,* **10,** 194–204.

Baik, J.-J., 1992: Response of a stably stratified atmosphere to low-level heating—An application to the heat island problem. *J. Appl. Meteor.,* **31,** 291–303.

Barcilon, A., J. C. Jusem, and S. Blumsack, 1980: Pseudo-adiabatic flow over a two-dimensional ridge. *Geophys. Astrophys. Fluid Dyn.,* **16,** 19–33.

Bluestein, H. B., and M. H. Jain, 1985: Formation of mesoscale lines of precipitation: Severe squall lines in Oklahoma during spring. *J. Atmos. Sci.,* **42,** 1711–1732.

Booker, J. R., and F. P. Bretherton, 1967: The critical layer for internal gravity waves in a shear flow. *J. Fluid Mech.,* **27,** 513–539.

Bretherton, C., 1988: Group velocity and the linear response of stratified fluids to internal heat or mass sources. *J. Atmos. Sci.,* **45,** 81–93.

Changnon, S. A., R. T. Shealy, and R. W. Scott, 1991: Precipitation changes in fall, winter, and spring caused by St. Louis. *J. Appl. Meteor.,* **30,** 126–134.

Chun, H.-Y., and J.-J. Baik, 1994: Weakly nonlinear response of a stably stratified atmosphere to diabatic forcing in a uniform flow. *J. Atmos. Sci.,* **51,** 3109–3121.

——, and Y.-L. Lin, 1995: Enhanced response of an atmospheric flow to a line-type heat sink in the presence of a critical level. *Meteor. Atmos. Phys.,* **55,** 33–45.

Droegemeier, K. K., and R. B. Wilhelmson, 1987: Numerical simulation of thunderstorm outflow dynamics. Part I: Outflow sensitivity experiments and turbulence dynamics. *J. Atmos. Sci.,* **44,** 1180–1210.

Eliassen, A., and E. Palm, 1960: On the transfer of energy in stationary mountain waves. *Geophys. Publ.,* **22,** 1–23.

Fraser, A. B., R. Easter, and P. Hobbs, 1973: A theoretical study of the flow of air and fallout of solid precipitation over mountainous terrain. Part I: Airflow model. *J. Atmos. Sci.,* **30,** 813–823.

Garstang, M., P. D. Tyson, and G. D. Emmitt, 1975: The structure of heat islands. *Rev. Geophys. Space Phys.,* **13,** 139–165.

Hooke, W. H., 1988: Gravity waves. *Mesoscale Meteorology and Forecasting,* P. S. Ray, Ed., Amer. Meteor. Soc., 272–288.

Lin, Y.-L., 1987: Two-dimensional response of a stably stratified shear flow to diabatic heating. *J. Atmos. Sci.,* **44,** 1375–1393.

——, 1994: Airflow over mesoscale heat sources. Part I: Responses in a uniform flow. *Proc. Natl. Sci. Counc. ROC(A),* **18,** 1–32.

——, and R. B. Smith, 1986: Transient dynamics of airflow near a local heat source. *J. Atmos. Sci.,* **43,** 40–49.

——, and R. C. Goff, 1988: A study of a mesoscale solitary wave in the atmosphere originating near a region of deep convection. *J. Atmos. Sci.,* **45,** 194–205.

——, and S. Li, 1988: Three-dimensional response of a shear flow to elevated heating. *J. Atmos. Sci.,* **45,** 2987–3002.

——, and H.-Y. Chun, 1991: Effects of diabatic cooling in a shear flow with a critical level. *J. Atmos. Sci.,* **48,** 2476–2491.

Nicholls, M. E., R. A. Pielke, and W. R. Cotton, 1991: Thermally forced gravity waves in an atmosphere at rest. *J. Atmos. Sci.,* **48,** 1869–1884.

Ogura, Y., and M.-T. Liou, 1980: The structure of a midlatitude squall line: A case study. *J. Atmos. Sci.,* **37,** 553–567.

Olfe, D. B., and R. L. Lee, 1971: Linearized calculations of urban heat island convection effects. *J. Atmos. Sci.,* **28,** 1374–1388.

Pandya, R., and D. R. Durran, 1996: The influence of convectively generated thermal forcing in the mesoscale circulation around squall lines. *J. Atmos. Sci.,* **53,** 2924–2951.

——, ——, and C. Bretherton, 1993: Comments on ''Thermally forced gravity waves in an atmosphere at rest.'' *J. Atmos. Sci.,* **50,** 4097–4101.

Raymond, D. J., 1986: Prescribed heating of a stratified atmosphere as a model for moist convection. *J. Atmos. Sci.,* **43,** 1101–1111.

Smith, R. B., and Y.-L. Lin, 1982: The addition of heat to a stratified airstream with application to the dynamics of orographic rain. *Quart. J. Roy. Meteor. Soc.,* **108,** 353–378.

Wyss, J., and K. A. Emanuel, 1988: The pre-storm environment of midlatitude prefrontal squall lines. *Mon. Wea. Rev.,* **116,** 790–794.

Yang, M.-J., and R. A. Houze Jr., 1995: Multicell squall-line structure as a manifestation of vertically trapped gravity waves. *Mon. Wea. Rev.,* **123,** 641–661.